Photosynthesis Research (2023) 156:205–215
https://doi.org/10.1007/s11120-023-01004-2

RESEARCH

Temperature sensitivity of carbon concentrating mechanisms in the diatom *Phaeodactylum tricornutum*

Meng Li[1] · **Jodi N. Young**[1]

Received: 30 November 2022 / Accepted: 10 February 2023 / Published online: 7 March 2023

Abstract

Marine diatoms are key primary producers across diverse habitats in the global ocean. Diatoms rely on a biophysical carbon concentrating mechanism (CCM) to supply high concentrations of CO_2 around their carboxylating enzyme, RuBisCO. The necessity and energetic cost of the CCM are likely to be highly sensitive to temperature, as temperature impacts CO_2 concentration, diffusivity, and the kinetics of CCM components. Here, we used membrane inlet mass spectrometry (MIMS) and modeling to capture temperature regulation of the CCM in the diatom *Phaeodactylum tricornutum (Pt)*. We found that enhanced carbon fixation rates by *Pt* at elevated temperatures were accompanied by increased CCM activity capable of maintaining RuBisCO close to CO_2 saturation but that the mechanism varied. At 10 and 18 °C, diffusion of CO_2 into the cell, driven by *Pt*'s 'chloroplast pump' was the major inorganic carbon source. However, at 18 °C, upregulation of the chloroplast pump enhanced (while retaining the proportion of) both diffusive CO_2 and active HCO_3^- uptake into the cytosol, and significantly increased chloroplast HCO_3^- concentrations. In contrast, at 25 °C, compared to 18 °C, the chloroplast pump had only a slight increase in activity. While diffusive uptake of CO_2 into the cell remained constant, active HCO_3^- uptake across the cell membrane increased resulting in *Pt* depending equally on both CO_2 and HCO_3^- as inorganic carbon sources. Despite changes in the CCM, the overall rate of active carbon transport remained double that of carbon fixation across all temperatures tested. The implication of the energetic cost of the *Pt* CCM in response to increasing temperatures was discussed.

Keywords Diatom · CCM · Temperature · Modeling · RuBisCO · *Phaeodactylum tricornutum*

Introduction

Diatoms are responsible for 40% of marine carbon fixation (Field et al. 1998) and are found across all latitudes of the ocean. Increasing anthropogenic inputs of CO_2 into the atmosphere is driving both ocean warming and an increase in the ocean's absorption of anthropogenic CO_2 leading to decreasing oceanic pH (ocean acidification) and changes in oceanic carbon chemistry with increasing concentrations of dissolved CO_2 and HCO_3^- (Zeebe 2012; Cheng et al. 2022). While different marine phytoplankton species have differing responses to the elevation of CO_2 (Dutkiewicz et al. 2015), diatoms' ability to fix carbon appears largely insensitive to ocean acidification due to their highly effective carbon concentrating mechanisms (CCMs) that can utilize the much larger pool of HCO_3^- available in seawater. Most diatoms studied to date possess a biophysical CCM that uses a compartment (pyrenoid) capable of elevating CO_2 around the CO_2 fixing enzyme, RuBisCO (Roberts et al. 2007; Hopkinson et al. 2016). Some diatoms may also possess a biochemical CCM (e.g., a C4 pathway) but this is still open for debate (Reinfelder et al. 2000; Morel et al. 2002; Roberts et al. 2007; Clement et al. 2016) and is not the focus of this study. While pyrenoids are common in diatoms, the mechanism by which the CCM elevates CO_2 around RuBisCO varies among species. Broadly, there appears to be two types of CCM, (1) those where inorganic carbon (C_i) uptake is dependent on an extracellular carbonic anhydrase (eCA) and (2) those lacking an eCA and instead rely on HCO_3^- transporters on the cell membrane for C_i uptake (Tsuji et al. 2017a).

While algal CCMs are highly effective, they are also energy intensive (Raven 2010; Raven et al. 2014). CCMs elevate pyrenoid CO_2 concentrations (needed to nearly saturate RuBisCO) to levels that far exceed CO_2

✉ Jodi N. Young
youngjn@uw.edu

[1] School of Oceanography, University of Washington, Seattle, WA, USA

concentrations in seawater, creating large concentration gradients, which encourages diffusive CO_2 efflux across highly permeable membranes. Manipulation of internal CO_2 pools and active transport of HCO_3^- across membranes requires energy input. Numerous studies have shown that increased extracellular CO_2 or changes in extracellular or intracellular pH can reduce the energetic requirement of the CCM (Hopkinson 2014; Mangan et al. 2016), however, there has been mixed evidence in diatoms on whether this can result in enhanced carbon fixation rates (Gao et al. 2014). Optimal CCM function requires synergistically balancing different CCM components, which facilitate HCO_3^- and CO_2 influx into the cell, recycling of leaked CO_2 and the maintenance of high CO_2 concentrations inside the pyrenoid.

Temperature plays a large but relatively understudied role on the CCM. As temperatures increase, the solubility of CO_2 and O_2 in seawater is reduced, along with a decrease in RuBisCO substrate affinity and CO_2/O_2 specificity (Galmés et al. 2016). However, membrane permeability, rates of diffusion and biochemical reaction rates all increase with rising temperatures, until an optimum is reached (Beardall et al. 2009; Li and Young 2022). It is likely that the temperature sensitivity of these different CCM components vary, leading to imbalanced C_i fluxes with fluctuating temperature. Therefore, diatoms need to regulate their CCM components to maintain balanced C_i fluxes to support high photosynthetic efficiency. There has been extensive research on the response of C4 plants (biochemical CCM) to varying temperature (Sage and Kubien 2007) but little is known about CCM response to temperature in the marine environment. While temperature fluctuations may not be as large in marine compared to terrestrial environments, marine heatwaves can be 5–6 °C above average temperatures and are devastating for marine ecosystems (Frölicher and Laufkötter 2018). It is likely these marine heatwaves are becoming more common, particularly in coastal regions (Lima and Wethey 2012; Hughes et al. 2018).

Phaeodactylum tricornutum (*Pt*) is a model coastal marine diatom with a well-established CCM model at 20 °C (Hopkinson et al. 2011; Hopkinson 2014). While *Pt* is of low abundance in the open ocean, it is widely distributed globally from sub-polar to tropical environments and able to grow between 5 and 28 °C in the lab (Kudo et al. 2000; De Martino et al. 2011; Rastogi et al. 2020). Here, we acclimated the model diatom *Pt* to three different temperatures over its growth range and measured CCM activity using membrane inlet mass spectrometry (MIMS). Experimental data were fit within the *Pt* CCM model, based on *Fragilariopsis cylindrus* (*Fcyl*) CCM (Li and Young 2022) adapted from the "chloroplast pump" model (Hopkinson 2014), to explore how the *Pt* CCM functions across temperatures.

Materials and methods

Cell culture conditions and growth rate

Phaeodactylum tricornutum CCMP632 (*Pt*) cells were cultured in buffered (25 mM HEPES, pH 8.10) f/2 media with salinity at 35‰. The pH of the culture media was adjusted to 8.10 for each growth temperature, i.e., 10 °C, 18 °C and 25 °C. Light intensity was set at ~ 120 µmol m^{-2} s^{-1} with 16 h:8 h, light:dark cycle. Cell cultures were subcultured weekly and acclimated at each temperature for at least two weeks. Initial inoculum was 1×10^4 cells ml^{-1} (or 1×10^5 cells ml^{-1} at 10 °C) at day zero and cells were harvested during exponential growth phase, at cell densities between 5×10^5 and 1×10^6 cells ml^{-1} on the day of each experiment. Growth rates were calculated as described in Li and Young (2022). Beckman Coulter Z2 cell counter was used to determine cell density and size, assuming a spherical cell shape for diameter calculation. The nonspherical shape of *Pt* cells, which determines the cell surface area, does not impact the estimation of volume-based mass transfer coefficients.

Membrane inlet mass spectrometry

Membrane Inlet Mass Spectrometry (MIMS), including gas concentration calibrations and data analyses are as described in Li and Young (2022) for *Fcyl*. Photosynthesis and C_i usage measurements with *Pt* cells were carried out in a similar fashion though at different temperatures (10, 18 and 25 °C) with the presence of the eCA inhibitor acetazolamide (AZ) as detailed in previous studies (Hopkinson et al. 2011; Hopkinson 2014; Li and Young 2022). Like our *Fcyl* experiments, ^{18}O, ^{13}C-labeled $NaHCO_3$ (final concentration ~ 2 mM) was used to determine HCO_3^- dehydration rate, CO_2/HCO_3^- mass transfer coefficient (f_c, f_b) and CA activities at different temperatures (Li and Young 2022). *Pt* cells were concentrated before loading into the MIMS chamber with final average densities of $3 \sim 4 \times 10^6$ cells ml^{-1}.

Photosynthetic rate and C_i uptake versus DIC concentration

Additional experiments to investigate the apparent kinetic properties of *Pt* C_i uptake were conducted by measuring rates of O_2 evolution under varying dissolved inorganic carbon concentrations ([DIC]). Similar to the previous study of Hopkinson (2014), stepwise increases in [DIC] were created by loading ^{13}C-$NaHCO_3$ into the MIMS chamber in the presence of 25 mM HEPES buffered (pH 8.1) artificial seawater. For each different [DIC], *Pt* cells were treated to a dark–light-dark cycle until quasi-steady state was reached

(see Fig. S1, e.g.). The CO_2 and O_2 signals were used for calculating photosynthetic rate and Ci uptake according to earlier studies (Badger et al. 1994; Hopkinson et al. 2011; Li and Young 2022). The cytosolic CO_2 concentration was estimated using following equation:

$$[CO_2]_{cyt} = [CO_2]_{bulk} - \frac{U_{CO_2}}{f_c} \quad (1)$$

where $[CO_2]_{cyt}$ and $[CO_2]_{bulk}$ are the cytosolic and bulk CO_2 concentrations respectively; U_{CO2} is the CO_2 uptake rate and f_c is the mass transfer coefficient of CO_2. The rate of photosynthesis (O_2 evolution) as a function of $[CO_2]$ was plotted and fit to the Michaelis–Menten equation.

RuBisCO kinetics and quantification

In vitro RuBisCO kinetics at different temperatures (6, 12, 18, 25 °C) were measured according to previous studies (Sharwood et al. 2008; Young et al. 2016). Briefly, RuBisCO active sites were quantified using [^{14}C] 2-CABP binding assay as described by Sharwood et al. (2008). For the ribulose-P_2-dependent $^{14}CO_2$-fixation assays, crude extracts of soluble diatom protein were incubated with 15 mM $NaH^{14}CO_3$ and 15 mM $MgCl_2$ at the relevant temperature for 10–15 min to activate RuBisCO. This extract was added to 7 ml septum-capped scintillation vials containing reaction buffer (0.5 ml of 100 mM EPPS-NaOH, pH 8, 15 mM $MgCl_2$, 0.6 mM ribulose-P_2, 0.1 mg ml^{-1} CA) equilibrated with 21% (v/v) O_2 in N_2 and five differing concentrations of $^{14}CO_2$ (between 10 and 115 µM). Values for the half saturation constant for CO_2 in air (K_{Cair}) and maximal carboxylase activity in air (V_{Cmax}) were extrapolated from the data using the Michaelis–Menten equation as described previously (Sharwood et al. 2008; Whitney et al. 2011). The carboxylation turnover rate of RuBisCO (k_{catC}) was calculated by dividing V_{Cmax} by the number of RuBisCO active sites as determined in [^{14}C] 2-CABP-binding assay.

Temperature dependence of k_{catC} and K_{Cair} was described by fitting following equation as described by Arcus et al. (2016):

$$lnk = a \times lnT + b \times \left(\frac{1}{T}\right) + c \quad (2)$$

The best-fit constants (a, b, c) were used to interpolate k_{catC} and K_{Cair} values at different temperature (T).

Western Blots were used to quantify the relative abundance of RuBisCO in *Pt* cells cultured at different temperatures, with experimental details described previously (Li and Young 2022). However, Western Blots using commercial anti-RbcL antibody and standards consistently underestimated absolute RuBisCO concentrations in diatoms. Thus, for modeling purposes, average RuBisCO quantities were estimated by assuming *Pt* RuBisCO reaches 80% saturation rate during photosynthesis at 18 °C, based on previous modeling and field research work (Hopkinson 2014, Kranz et al. 2015).

Modeling and statistical analyses

We previously adapted the "chloroplast pump" models (Hopkinson 2014; Li and Young 2022) to simulate the C_i fluxes of *Fcyl*. By adjusting the HCO_3^- uptake behavior observed in our *Pt* data, as well as other physiochemical parameters acquired in this study, we modified the *Fcyl* CCM model to simulate *Pt* C_i fluxes during steady state photosynthesis at different temperatures. The model was constrained to describe observed CO_2 concentrations, net O_2 evolution rates and C_i uptake rates. The Python script with modeling parameter files can be found on GitHub (https://github.com/limengwsu/Pt_CCM_T). All descriptive statistical analyses including mean, stand deviation, tukey HSD p values, etc. were calculated using Python packages including pandas, numpy, scipy (Virtanen et al. 2020) and statsmodels (Seabold and Perktold 2010).

Results

Growth rates and photosynthesis with temperature

Pt net photosynthesis increased steadily across all temperatures tested, with an ~ fourfold increase between 10 and 25 °C, as measured by the rate of O_2 evolution in the light (Fig. 1a). Respiration (O_2 consumption in the dark) also increased significantly at 25 °C compared with 10 and 18 °C ($p \leq 0.001$, Fig. 1b). The estimated daily net O_2 evolution (calculated as 1/3 dark respiration and 2/3 light O_2 evolution over a 16:8 daylight cycle), increased with temperature ($p \leq 0.001$, Fig. 1c). However, the specific growth rate (d^{-1}) of *Pt* only increased between 10 and 18 °C, not between 18 and 25 °C (Fig. 1c). This disparity could be attributed to changing rates of respiration and photosynthesis over a diel cycle that were not captured in our short-term MIMS experiments. In addition, cell size also increased significantly between 18 and 25 °C ($p \leq 0.001$), though only by ~ 10% in volume, and may partly explain the difference observed between daily net photosynthesis and growth rates (Figs. 1c, S2).

RuBisCO kinetics and quantity

Faster growth and photosynthetic rates at higher temperatures could be attributed to the temperature-driven increase in RuBisCO catalytic activity (k_{catC}). From 10 to 25 °C, RuBisCO k_{catC} increased from 0.9 to 3.3 s^{-1}, an almost

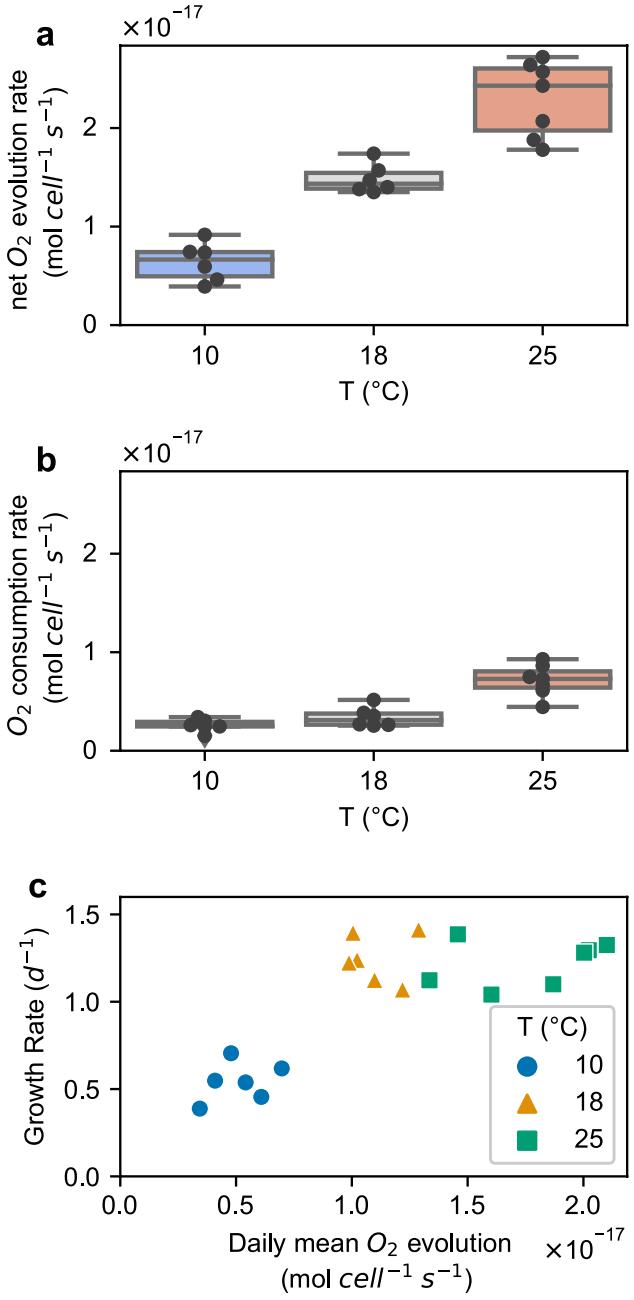

Fig. 1 *Pt* net photosynthetic, respiratory and growth rate at different temperature. **a.** Net oxygen evolutionary rate in the light per cell across different temperatures. **b.** Oxygen consumption (dark respiratory) rate per cell across different temperatures. **c.** The correlation between growth rate and averaged daily primary production rate, presented as daily net O_2 evolution rate per cell. All box plots have whiskers extending maximum 1.5 times of IQR from box

four-fold increase between 10 and 25 °C, similar in magnitude to the increase in photosynthetic oxygen evolution (Fig. 2a). Between 10 and 25 °C, there is also a 2.5-fold increase in K_{Cair} from 22 to 55 µM (Fig. 2a), thus at higher temperatures RuBisCO needs a higher CO_2 concentration for similar saturation levels. As K_{Cair} was less temperature sensitive than k_{catC}, carboxylation efficiency (k_{catC}/K_{Cair}) increases with temperature.

There was little change in RuBisCO abundance per cell across temperatures in *Pt* (Figs. 2b, S3a). The Western Blot method tracks changes in relative abundance but appears to underestimate diatom RbcL quantity in *Pt*, which was also observed in our previous work on *Fcyl* (Li and Young 2022). Our estimation of average gross CO_2 fixation rates at RuBisCO (based on estimated gross O_2 evolution rates, Fig. S3b), increased from 0.90 to 3.0×10^{-17} mol cell^{-1} s^{-1} with a temperature increase from 10 to 25 °C. Dividing the gross CO_2 fixation rates by k_{catC}, the results lead to an average minimum RuBisCO quantity at 1×10^{-17} mol per *Pt* cell. For modeling purposes and to estimate the relative substrate (CO_2) concentration at RuBisCO, 80% saturation was assumed at 18 °C, which resulted in an estimated abundance of 1.24×10^{-17} mol RuBisCO per *Pt* cell across different temperatures. Combined with K_{Cair} data, we estimated the average CO_2 concentration around RuBisCO during steady state photosynthesis to be 95, 147, and 151 µM at 10, 18, and 25 °C, respectively.

Inorganic carbon usage

An increase in cellular inorganic carbon (C_i) uptake was required to supply the faster carboxylation rates and maintain higher CO_2 concentrations within the pyrenoid with increasing temperature. Total C_i uptake increases at higher temperatures, which was largely driven by an increase in CO_2 uptake from 10 to 18 °C (Fig. 3a) and by an increase in HCO_3^- uptake from 18 to 25 °C (Fig. 3b). This results in the proportional supply of C_i in *Pt* to be ~ 80% CO_2 at the lower temperatures of 10 and 18 °C, but only ~ 50% CO_2 supply at 25 °C ($p \le 0.006$, Fig. 3c).

Using ^{18}O-exchange method (Hopkinson et al. 2011; Li and Young 2022), we estimated the mass transfer coefficients of CO_2 and HCO_3^- (f_c, f_b respectively) in *Pt* at different temperatures. The permeability of CO_2 across the *Pt* cell membrane (and frustule), measured as f_c, steadily increased with temperature ($p \le 0.006$ for each temperature pair, Fig. 4a). The permeability for HCO_3^-, indicated by f_b, was three orders of magnitude lower than CO_2 and insensitive to temperature (Fig. 4a). Thus, as noted in previous studies (Hopkinson et al. 2011), the cell membrane can be treated as essentially impermeable for HCO_3^-. The increased f_c at higher temperatures may facilitate the influx of CO_2, where CO_2 uptake rates are faster at higher temperatures than at 10 °C ($p \le 0.007$, Fig. 3b). As discussed by Hopkinson (2014), the cytosolic CA can also facilitate CO_2 uptake. Like f_c, the estimated catalytic rate of intracellular CA in *Pt* was higher at warmer temperatures ($p < 0.02$ for each temperature pair, Fig. 4b).

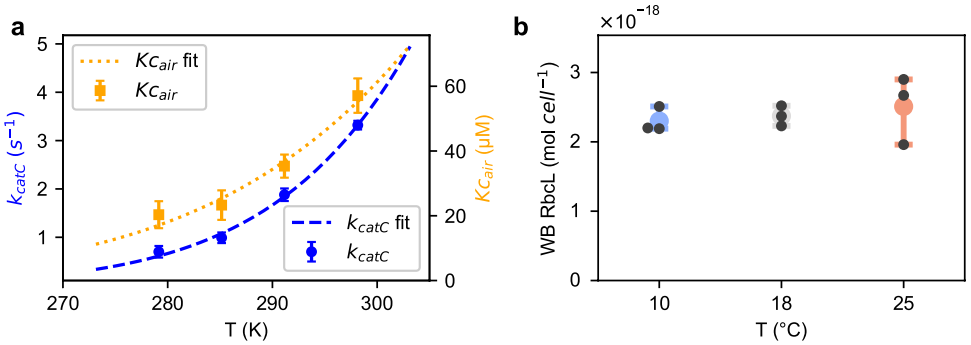

Fig. 2 The impact of temperature on RuBisCO kinetic properties and quantity in *Pt. a.* RuBisCO carboxylation kinetic parameters k_{catC} and K_{Cair} in the presence of air. Curve fitting and interpolation were used to derived parameters at different temperatures. **b.** Western Blot (WB) quantification of RbcL in *Pt* cultured at different temperatures. Error bars represent SD with $n = 3$

C_i uptake rate versus C_i concentration

To understand the kinetics of C_i uptake by *Pt* and to model C_i fluxes during photosynthesis at different temperatures, we investigated the effect of [DIC] on net photosynthetic rates (Fig. 5a). As expected, lower [DIC] limited net photosynthetic rates across different temperatures. However, when C_i uptake was analyzed, the limitation of photosynthesis was not from the limited HCO_3^- uptake under our experimental conditions. HCO_3^- uptake was not responsive to bulk [HCO_3^-] in the range of 0.08–2 mM, regardless of temperature (Fig. 5b). This indicates that *Pt* has highly specific HCO_3^- transporters that operate with half saturation constants ($K_{0.5}$) < < 100 μM (agreeing with earlier research on *Pt* (Nakajima et al. 2013; Tsuji et al. 2017a; Nawaly et al. 2022). The observed insensitivity of HCO_3^- uptake to bulk [HCO_3^-] (and [DIC]) suggests an alternative entry of C_i into the cytosol (Fig. S4), i.e., through CO_2 diffusion, which causes the limit on photosynthesis at low [DIC].

The diffusion of CO_2 into the cell is driven by the CO_2 concentration gradient between the extracellular environment and the cytosol (Hopkinson 2014). C_i from the cytosol is then concentrated within the chloroplast by the "chloroplast pump". The "chloroplast pump" as defined by Hopkinson (2014) intensively "pumps" HCO_3^- from the cytosol to the chloroplast, maintaining low HCO_3^- concentrations within the cytosol. Rapid cytosolic-CA-mediated net flux of CO_2 to HCO_3^- then drives the diffusive influx of CO_2 into the cytosol from outside the cell. With our measured f_c, we estimated cytosolic CO_2 concentrations using Eq. 1, which allowed us to investigate the relationship between cytosolic CO_2 concentration and net photosynthetic rate (Fig. S5b). Fitting the net O_2 evolution rate versus extracellular and cytosolic CO_2 concentrations to the Michaelis–Menten curve separately revealed a strong "chloroplast pump", with average $K_{0.5} \leq 1$ μM for both extracellular and cytosolic CO_2 (Fig. S5). With the equilibrium constant of CO_2/HCO_3^- interconversion being ~ 100, the $K_{0.5}$ for HCO_3^- transport from the cytosol to the chloroplast was estimated to be < 100 μM. With our experimental setup, the temperature impact on the affinity ($K_{0.5}$) of HCO_3^-/CO_2 at the chloroplast level was not distinguishable.

Modeling the CCM with temperature

Combining the quantitative data of RuBisCO kinetics, CA activities, net O_2 evolution, C_i uptake rates and its kinetic properties, etc., we modeled the C_i fluxes in *Pt* during photosynthesis at different temperatures (Fig. 6). At steady state in general, CO_2 diffuses from the bulk environment through the surface layer and cytoplasmic membrane into the cytosol, with additional CO_2 supplied to the cytosol from mitochondrial respiration and leakage from the chloroplast (gray arrows pointing at cytosolic CO_2, Fig. 6). The concentrations of CO_2 and HCO_3^- in the cytosol favor the net conversion of CO_2 to HCO_3^- by cytosolic CA. The CA supplied HCO_3^-, combined with extracellular HCO_3^- uptake through cytoplasmic membrane, is pumped into the chloroplast by potential transporter(s). This allows the accumulation of high concentrations of HCO_3^- within chloroplast and subsequently in the pyrenoid, where HCO_3^- is converted to CO_2 by pyrenoid CA and fixed by RuBisCO (green arrows, Fig. 6). Due to the concentration gradient between pyrenoid and chloroplast stroma, some proportion of the CO_2 leaks out from the pyrenoid into the chloroplast stroma and subsequently into the cytosol. As discussed by Hopkinson (Hopkinson 2014), the lack of CAs in the chloroplast stroma allows the buildup of HCO_3^-, with a very small fraction converted to CO_2 before reaching the pyrenoid.

As temperature increases, the model was able to capture the experimentally observed fluxes of C_i uptake and photosynthetic rates, including faster diffusive CO_2 uptake from the bulk environment to the cytosol at 18 °C compared with 10 °C, and enhanced HCO_3^- uptake into the cytosol at 25 °C

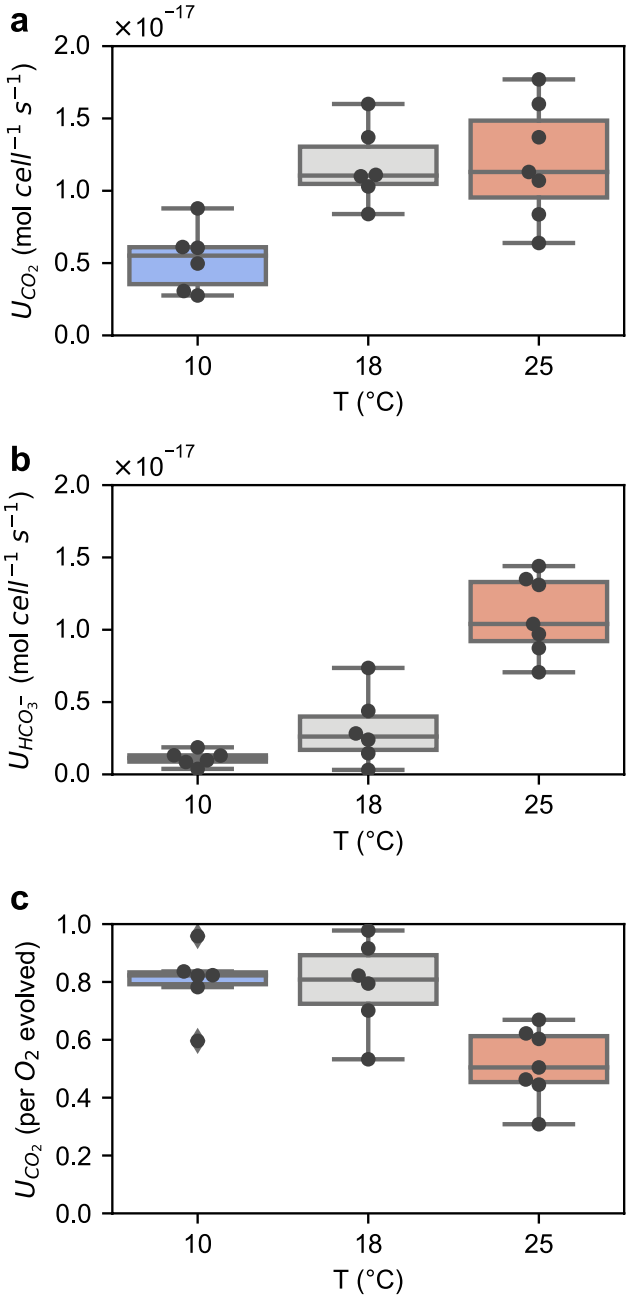

Fig. 3 Inorganic carbon uptake by *Pt* at different temperatures. *a* and **b** Uptake rate of CO_2 (U_{CO2}) and HCO_3^- (U_{HCO3-}) per cell basis. **c.** Fraction of CO_2 supply normalized to O_2 evolution

compared with 18 °C (Figs. 3, 6). The model also enabled visualization of the intracellular C_i fluxes that are less accessible through experiments. All intracellular C_i fluxes operate at faster rates as temperatures rise (Fig. 6). Notably the net fluxes of cytosolic CA-catalyzed conversion of CO_2 to HCO_3^-, HCO_3^- transport from the cytosol to the chloroplast, and the leakage of CO_2 from the chloroplast to the cytosol are faster at higher temperatures. For every mole of HCO_3^- transported into the chloroplast, there are 0.37, 0.45, and 0.43 mol of CO_2 leaking out of the chloroplast at 10, 18, and 25 °C, respectively. In other words, for every carbon fixed by RuBisCO, there are 1.6, 1.8 and 1.8 HCO_3^- molecules transported into the chloroplast at 10, 18, and 25 °C, respectively. When HCO_3^- uptake from the surface/bulk environment into the cytosol is included (i.e., total active HCO_3^- transport), the ratio of active HCO_3^- transport to carboxylation rate at RuBisCO is approximately 2:1 for all three temperatures. The HCO_3^- concentrations within the chloroplast are ~ 20 times of that within cytosol at 10 °C, and ~ 40 times at 18 and 25 °C. This is the result of cytosolic HCO_3^- concentrations remaining ~ 0.7 mM across all temperatures, whereas the chloroplast HCO_3^- concentration increased from 15 mM at 10 °C to ~ 30 mM at 18 and 25 °C.

Discussion

The CCM of *Pt* is essential to supply elevated CO_2 concentrations around RuBisCO (Hopkinson et al. 2011; Hopkinson 2014). While there has been much focus on the response of diatom carbon fixation to ocean acidification (Wu et al. 2014; Shi et al. 2019; Wada et al. 2021), less is known about how marine heatwaves and rising sea surface temperatures (SST) may impact the diatom CCM and ultimately the ability of diatoms to sequester carbon.

CCM activity increases with temperature

Our experimental conditions of nutrient replete, saturating light resulted in increasing carbon fixation rates in *Pt* as temperatures increased. Concomitantly, there was also an increase in CCM activity to support the increased demand of CO_2 for fixation, overcoming the challenges at higher temperatures of lower CO_2 solubility in the bulk medium, higher half saturation constants for CO_2 by RuBisCO and lower CO_2/O_2 specificity of RuBisCO (Galmés et al. 2016). Increased activity of the CCM occurred due to an overall increase in catalytic rates of CAs and HCO_3^- transporters, as well as enhanced membrane permeability to CO_2 and increased rates of CO_2 diffusion. As temperatures increased, we observed a shift towards a larger proportion of HCO_3^- to CO_2 uptake from the bulk media, and a slight lowering of RuBisCO saturation state (from 81 to 73%). Modeling of the CCM revealed that *Pt* initially increased CO_2 supply to RuBisCO by enhancing its "chloroplast pump" (from 10 to 18 °C). This involved increasing HCO_3^- transport across the chloroplast membranes. The rapid removal of inorganic carbon from the cytosol was quickly replaced by predominantly diffusive entry of CO_2 but also active HCO_3^- uptake into the cell. The ratio of cellular CO_2: HCO_3^- uptake did not change between 10 and 18 °C (Fig. 3c). However, between 18 and 25 °C it appeared that the "chloroplast pump" cannot

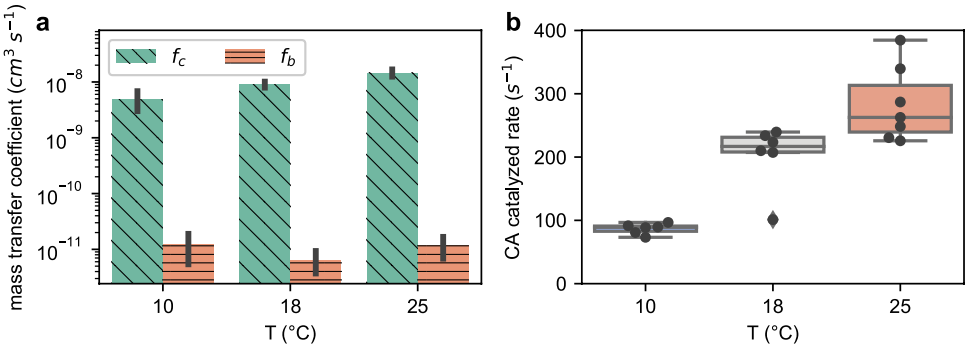

Fig. 4 Temperature impact on *Pt* inorganic carbon mass transfer coefficient (**a**) and intracellular CA catalytic rate (**b**)

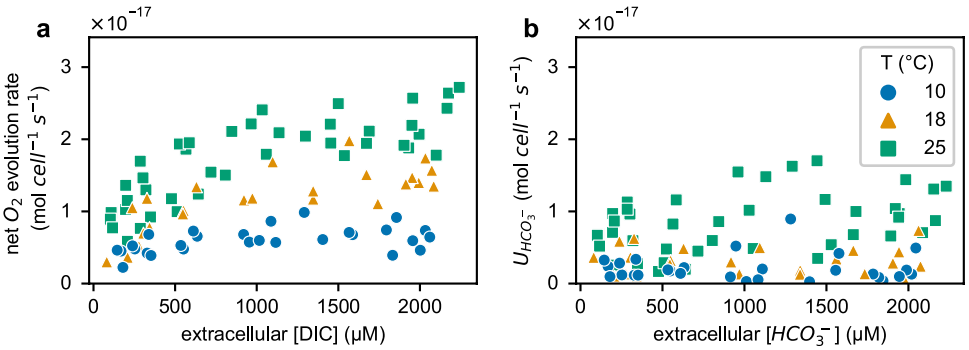

Fig. 5 The impact of DIC (**a**) and HCO_3^- (**b**) concentration on net O_2 evolution rate and uptake rate of HCO_3^- respectively. Data points were pooled from 4, 3, 5 independent cultures for temperature at 10, 18, 25 °C respectively

be further enhanced, either unable to elevate chloroplast HCO_3^- concentrations above 30 mM or unable to maintain a chloroplast-to-cytosol HCO_3^- gradient greater than ~ 40 fold. Once this limit had been reached, the increased demand for inorganic carbon was supplied by enhancing the uptake of HCO_3^- from the bulk media. A comparable intracellular HCO_3^- concentration ~ 30 mM has been estimated in cyanobacteria previously (Woodger et al. 2005; Mangan and Brenner 2014).

Temperature effects on kinetics or molecular regulation on CCM components?

As temperature increases, catalytic activity, diffusion rates, and membrane fluidity also increase until an optimum is reached. Observed increased rates of CA activity, HCO_3^- transport, and CO_2 carboxylation at RuBisCO are of magnitudes that could be explained by the direct impact of temperature (for enzymes assuming a Q_{10} around 2) without changes in enzyme abundance. Likewise, the differences in the magnitudes of various C_i fluxes (Fig. 6b, c) between 10 and 18 °C could also be entirely due to different temperature sensitivities of CCM components. However, at 25 °C the shifted ratio of CO_2 to HCO_3^- uptake fluxes (Fig. 6a) and the upheld saturation state of RuBisCO suggest that there is a temperature-driven physiological and molecular regulation of CCM components. Further investigations (e.g., transcriptional studies) beyond our current model are needed to test whether *Pt* regulates its CCM through gene expression in response to changing temperatures. Previous studies have demonstrated that CCM components (e.g., CA, HCO_3^- transporters) are transcriptionally regulated via CO_2 availability (Harada et al. 2006; Ohno et al. 2012; Nakajima et al. 2013; Hennon et al. 2015) indicating that the CCM is dynamically able to respond to changing environmental conditions.

Temperature impacts on the energy cost of the *Pt* CCM

The energetic cost of the CCM is thought to be primarily driven by the active uptake of HCO_3^- across membranes and to be strongly correlated with the amount of CO_2 leaked from the pyrenoid. While CO_2 leaks from the pyrenoid and chloroplast in the *Pt* CCM model, it is recycled in the cytosol by CA into HCO_3^-. This "chloroplast pump" model in *Pt* (Hopkinson et al. 2011; Hopkinson 2014) revealed the dependence on active pumping of HCO_3^- from the cytosol into the chloroplast to maintain a low cytosolic CO_2 concentration. This low cytosolic CO_2 concentration drives the net influx of CO_2 from the bulk environment into the cytosol, along with rapid recycling of CO_2 respired from the mitochondria or leaked from the chloroplast. Below we discuss the energy costs of this model in the context of temperature but acknowledge that other diatoms have different CCM strategies such as relying on external CA for extracellular HCO_3 uptake while CO_2 could leak from the cell (Tsuji et al. 2017a; Li and Young 2022).

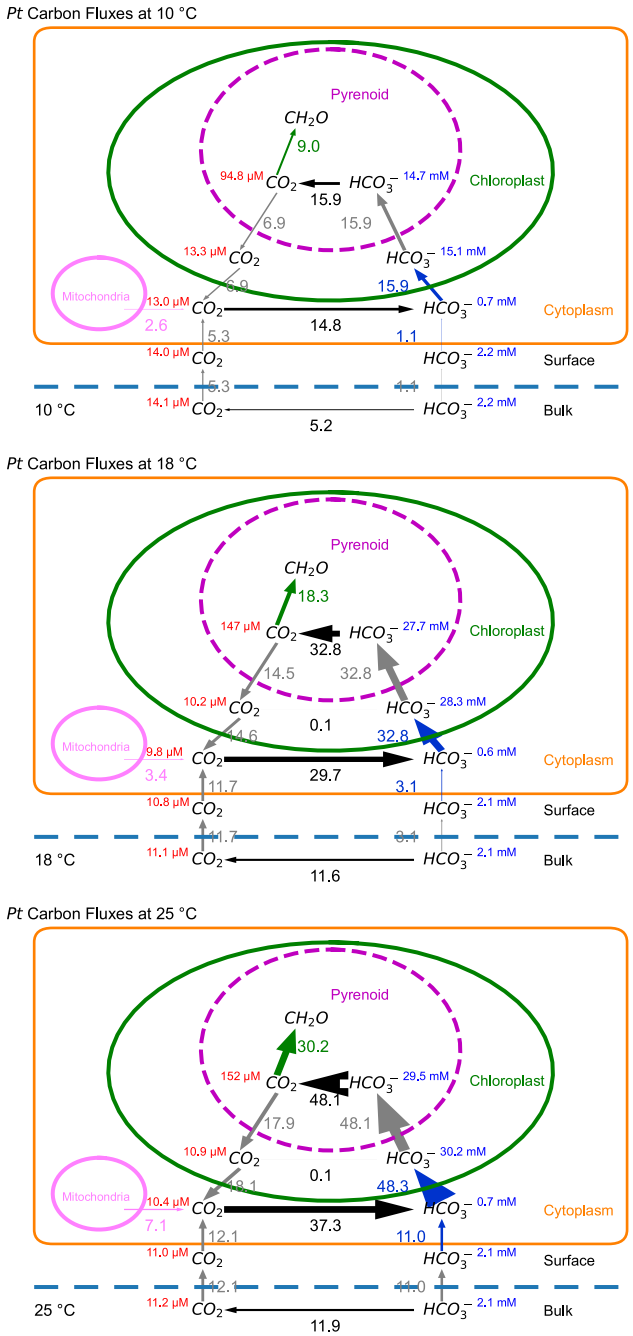

Fig. 6 CCM models of *Pt* carbon (Ci) fluxes during photosynthesis at different temperatures. Gray, black, blue, and green arrows along with net flux rates (unit in 10^{-18} mol cell^{-1} s^{-1}) represent diffusive, interconversion, active uptake, and fixation of inorganic carbon species, respectively. Arrow widths are drawn proportional to flux rates. The concentrations of CO_2 and HCO_3^- are labeled in each compartment with units. The "Surface" compartment (Hopkinson et al. 2013) denotes the cellular layer outside the cytoplasmic membrane, including periplasmic space and frustule

Active transport of HCO_3^- across the cytoplasmic membrane in *Pt* is done by the Na^+-dependent SLC4-type transporters while the "chloroplast pump" HCO_3^- transporters are yet to be identified (Nakajima et al. 2013; Tsuji et al. 2017b; Nawaly et al. 2022). Without direct measurements, HCO_3^- transport across the plasmalemma or chloroplast envelope membranes was estimated to require 0.5 or 1 ATP for each HCO_3^- transported (Hopkinson et al. 2011; Raven et al. 2014). Considering the HCO_3^- concentration gradient between the chloroplast and cytosol was ~ 40 fold at maximum (Fig. 6), and factoring in the ~ 20 mV chloroplast envelope membrane potential under light (Demmig and Gimmler 1983; Pottosin and Dobrovinskaya 2015), the energy input required would be ~ 11 kJ/mol HCO_3^- transported from the cytosol to the chloroplast stroma, which is considerably lower than the −51 kJ/mol for the hydrolysis of ATP (estimated from chloroplast ATP/ADP concentrations (Heineke et al. 1991)). This indicates that a relatively energy efficient "chloroplast pump" is possible, so the estimate of 0.5 ATP for each HCO_3^- transported can hold. In contrast to HCO_3^- transport into the chloroplast, the cytoplasmic uptake of HCO_3^- has a favorable concentration gradient, i.e., the cytosolic HCO_3^- concentration is lower than the bulk environment. This favorable concentration gradient, together with the unfavorable cytoplasmic membrane potential −84 mV (resting potential, oscillating up to −40 mV) measured from the diatom *Odontella sinensis* (Taylor 2009), points to an estimated energy requirement of ~ 5.5 kJ/mol for HCO_3^- transport across the cytoplasmic membrane into the cytosol. Thus, HCO_3^- transporters (such as the SLC4-type) on the cytoplasmic membrane can operate efficiently using 0.5 or less ATP per HCO_3^- uptake into the cytosol. The ratio of total active HCO_3^- transport to CO_2 fixed at RuBisCO remained at 2:1 across all temperatures (Fig. 6) indicating that the energy cost of the *Pt* CCM per CO_2 fixed does not change with temperature unless the energetic costs for chloroplast and cytoplasmic HCO_3^- uptake are different. Nevertheless, higher photosynthetic rates at higher temperatures (under nutrient replete conditions) will need a higher total energy input, requiring higher saturating light intensities.

In addition to the energetic cost of HCO_3^- transport, energy costs and resource allocation of the CCM must also take into consideration the synthesis and maintenance of the CCM biophysical components (Raven et al. 2014). To compensate for slow catalytic rates at cold temperatures, many CCM components and RuBisCO are likely increased in abundance (Young et al. 2015; Li and Young 2022), this would require a larger investment in resources, such as nitrogen. While the abundance of other CCM components were not directly measured in this study, RuBisCO abundance did not change with temperature.

Combined effects of increasing SST and ocean acidification

Climate change will lead to both increasing SST and lowering of ocean pH. While warming SST leads to lower solubility of CO_2 in seawater with a given pH, increasing atmospheric CO_2 leads to elevating dissolved CO_2 and HCO_3^- in the ocean, decreasing the oceanic pH (Zeebe 2012; Cheng et al. 2022). We hypothesized that the effect of rising temperatures would put additional pressure on the CCM, negating any relaxation of the CCM due to increasing CO_2 concentrations. Our study showed that *Pt* increases CCM activity with increasing temperature, maintaining RuBisCO saturation above 70%. However, the increase in CCM activity is in pace with faster carboxylation rates, so that the estimated cost of the CCM does not increase per carbon fixed. Our study was conducted under nutrient replete conditions over a temperature range that led to increased carbon fixation rates with temperature. Nutrient limitation is predicted to become more prevalent in conjunction with warming SST due to enhanced stratification and could counter any temperature-driven increases in growth rate (Marinov et al. 2010). How the CCM functions under higher temperatures when nutrient limitation restricts carbon fixation rates has yet to be elucidated though there is evidence of either the Calvin cycle or CCM being downregulated in phytoplankton under phosphate limitation (Beardall et al. 2005; Brembu et al. 2017). Our study also highlighted the dependence of HCO_3^- transport in *Pt*'s "chloroplast pump" and an upper limit of either chloroplast HCO_3^- concentrations or chloroplast-to-cytosol gradients. At this limit (above 18 °C in this study), the CCM is no longer sensitive to CO_2 availability and ocean acidification would not affect carbon fixation rates under these experimental conditions.

Supplementary Information The online version contains supplementary material available at https://doi.org/10.1007/s11120-023-01004-2.

Acknowledgements We would like to thank B. Hopkinson for extensive advice and training for conducting MIMS experiments, and for sharing his mathematical model. We would like to thank S. Whitney for measuring *Pt* RuBisCO kinetics in collaboration with JY.

Author contributions JY designed the experiments, ML carried out and optimized experiments, performed data analysis. JY and ML wrote the paper.

Funding JY and ML were supported by Simons Foundation Award 561645. JY was also supported by the Sloan Foundation Fellowship and NSF OPP 17445645.

Data availability The Python script for Pt CCM modeling is available on GitHub: https://github.com/limengwsu/Pt_CCM_T. The results summary table is available on Dryad: https://doi.org/10.5061/dryad.jdfn2z3fn and raw MIMS signal data files are available upon request to the corresponding author.

Declarations

Conflict of interest The authors have no relevant financial or non-financial interests to disclose.

References

Arcus VL, Prentice EJ, Hobbs JK et al (2016) On the temperature dependence of enzyme-catalyzed rates. Biochemistry 55:1681–1688. https://doi.org/10.1021/acs.biochem.5b01094

Badger MR, Palmqvist K, Yu J-W (1994) Measurement of CO2 and HCO3− fluxes in cyanobacteria and microalgae during steady-state photosynthesis. Physiol Plant 90:529–536. https://doi.org/10.1111/j.1399-3054.1994.tb08811.x

Beardall J, Roberts S, Raven JA (2005) Regulation of inorganic carbon acquisition by phosphorus limitation in the green alga chlorella emersonii. Can J Bot 83:859–864. https://doi.org/10.1139/b05-070

Beardall J, Stojkovic S, Larsen S (2009) Living in a high CO2 world: impacts of global climate change on marine phytoplankton. Plant Ecolog Divers 2:191–205. https://doi.org/10.1080/17550870903271363

Brembu T, Mühlroth A, Alipanah L, Bones AM (2017) The effects of phosphorus limitation on carbon metabolism in diatoms. Phil Trans R Soc B 372:20160406. https://doi.org/10.1098/rstb.2016.0406

Cheng L, von Schuckmann K, Abraham JP et al (2022) Past and future ocean warming. Nat Rev Earth Environ 3:776–794. https://doi.org/10.1038/s43017-022-00345-1

Clement R, Dimnet L, Maberly SC, Gontero B (2016) The nature of the CO2-concentrating mechanisms in a marine diatom, Thalassiosira pseudonana. New Phytol 209:1417–1427. https://doi.org/10.1111/nph.13728

De Martino A, Bartual A, Willis A et al (2011) Physiological and molecular evidence that environmental changes elicit morphological interconversion in the model diatom phaeodactylum tricornutum. Protist 162:462–481. https://doi.org/10.1016/j.protis.2011.02.002

Demmig B, Gimmler H (1983) Properties of the isolated intact chloroplast at cytoplasmic K+ concentrations 1: I: light-induced cation uptake into intact chloroplasts is driven by an electrical potential difference. Plant Physiol 73:169–174. https://doi.org/10.1104/pp.73.1.169

Dutkiewicz S, Morris JJ, Follows MJ et al (2015) Impact of ocean acidification on the structure of future phytoplankton communities. Nature Clim Change 5:1002–1006. https://doi.org/10.1038/nclimate2722

Field CB, Behrenfeld MJ, Randerson JT, Falkowski P (1998) Primary production of the biosphere: integrating terrestrial and oceanic

components. Science 281:237–240. https://doi.org/10.1126/science.281.5374.237
Frölicher TL, Laufkötter C (2018) Emerging risks from marine heat waves. Nat Commun 9:650. https://doi.org/10.1038/s41467-018-03163-6
Galmés J, Hermida-Carrera C, Laanisto L, Niinemets Ü (2016) A compendium of temperature responses of Rubisco kinetic traits: variability among and within photosynthetic groups and impacts on photosynthesis modeling. J Exp Bot 67:5067–5091. https://doi.org/10.1093/jxb/erw267
Gao K, Campbell DA, Gao K, Campbell DA (2014) Photophysiological responses of marine diatoms to elevated CO2 and decreased pH: a review. Functional Plant Biol 41:449–459. https://doi.org/10.1071/FP13247
Harada H, Nakajima K, Sakaue K, Matsuda Y (2006) CO2 sensing at ocean surface mediated by cAMP in a marine diatom. Plant Physiol 142:1318–1328. https://doi.org/10.1104/pp.106.086561
Heineke H, Riens B, Grosse H et al (1991) Redox transfer across the inner chloroplast envelope membrane. Plant Physiol. 95(4):1131–1137. https://doi.org/10.1104/pp.95.4.1131
Hennon GMM, Ashworth J, Groussman RD et al (2015) Diatom acclimation to elevated CO2 via cAMP signalling and coordinated gene expression. Nature Clim Change 5:761–765. https://doi.org/10.1038/nclimate2683
Hopkinson BM (2014) A chloroplast pump model for the CO2 concentrating mechanism in the diatom Phaeodactylum tricornutum. Photosynth Res 121:223–233. https://doi.org/10.1007/s11120-013-9954-7
Hopkinson BM, Dupont CL, Allen AE, Morel FMM (2011) Efficiency of the CO2-concentrating mechanism of diatoms. Proc Natl Acad Sci 108:3830–3837. https://doi.org/10.1073/pnas.1018062108
Hopkinson BM, Meile C, Shen C (2013) Quantification of extracellular carbonic anhydrase activity in two marine diatoms and investigation of its role. Plant Physiol 162:1142–1152. https://doi.org/10.1104/pp.113.217737
Hopkinson BM, Dupont CL, Matsuda Y (2016) The physiology and genetics of CO2 concentrating mechanisms in model diatoms. Curr Opin Plant Biol 31:51–57. https://doi.org/10.1016/j.pbi.2016.03.013
Hughes TP, Anderson KD, Connolly SR et al (2018) Spatial and temporal patterns of mass bleaching of corals in the Anthropocene. Science 359:80–83. https://doi.org/10.1126/science.aan8048
Kranz SA, Young JN, Hopkinson BM, et al (2015) Low temperature reduces the energetic requirement for the CO_2 concentrating mechanism in diatoms. New Phytologist 205:192–201. https://doi.org/10.1111/nph.12976
Kudo I, Miyamoto M, Noiri Y, Maita Y (2000) Combined Effects of temperature and iron on the growth and physiology of the marine diatom Phaeodactylum Tricornutum (bacillariophyceae). J Phycol 36:1096–1102. https://doi.org/10.1046/j.1529-8817.2000.99042.x
Li M, Young JN (2022) Extracellular carbonic anhydrase supports constitutive HCO3− Uptake in Fragilariopsis cylindrus regardless of temperature changes. Biorxiv. https://doi.org/10.1101/2022.09.08.507187
Lima FP, Wethey DS (2012) Three decades of high-resolution coastal sea surface temperatures reveal more than warming. Nat Commun 3:704. https://doi.org/10.1038/ncomms1713
Mangan NM, Brenner MP (2014) Systems analysis of the CO2 concentrating mechanism in cyanobacteria. eLife 3:e02043. https://doi.org/10.7554/eLife.02043
Mangan NM, Flamholz A, Hood RD et al (2016) pH determines the energetic efficiency of the cyanobacterial CO2 concentrating mechanism. Proc Natl Acad Sci 113:E5354–E5362. https://doi.org/10.1073/pnas.1525145113
Marinov I, Doney SC, Lima ID (2010) Response of ocean phytoplankton community structure to climate change over the 21st century: partitioning the effects of nutrients, temperature and light. Biogeosciences 7:3941–3959. https://doi.org/10.5194/bg-7-3941-2010
Morel FMM, Cox EH, Kraepiel AML et al (2002) Acquisition of inorganic carbon by the marine diatom Thalassiosira weissflogii. Funct Plant Biol 29:301–308. https://doi.org/10.1071/pp01199
Nakajima K, Tanaka A, Matsuda Y (2013) SLC4 family transporters in a marine diatom directly pump bicarbonate from seawater. Proc Natl Acad Sci 110:1767–1772. https://doi.org/10.1073/pnas.1216234110
Nawaly H, Matsui H, Tsuji Y et al (2022) Multiple plasma membrane SLC4s contribute to external HCO3- acquisition during CO2 starvation in the marine diatom Phaeodactylum tricornutum. J Exp Bot. https://doi.org/10.1093/jxb/erac380
Ohno N, Inoue T, Yamashiki R et al (2012) CO2-cAMP-responsive cis-elements targeted by a transcription factor with CREB/ATF-like basic zipper domain in the marine diatom phaeodactylum tricornutum. Plant Physiol 158:499–513. https://doi.org/10.1104/pp.111.190249
Pottosin I, Dobrovinskaya O (2015) Ion channels in native chloroplast membranes: challenges and potential for direct patch-clamp studies. Front Physiol 6:396. https://doi.org/10.3389/fphys.2015.00396
Rastogi A, Vieira FRJ, Deton-Cabanillas A-F et al (2020) A genomics approach reveals the global genetic polymorphism, structure, and functional diversity of ten accessions of the marine model diatom Phaeodactylum tricornutum. ISME J 14:347–363. https://doi.org/10.1038/s41396-019-0528-3
Raven JA (2010) Inorganic carbon acquisition by eukaryotic algae: four current questions. Photosynth Res 106:123–134. https://doi.org/10.1007/s11120-010-9563-7
Raven JA, Beardall J, Giordano M (2014) Energy costs of carbon dioxide concentrating mechanisms in aquatic organisms. Photosynth Res 121:111–124. https://doi.org/10.1007/s11120-013-9962-7
Reinfelder JR, Kraepiel AML, Morel FMM (2000) Unicellular C4 photosynthesis in a marine diatom. Nature 407:996–999. https://doi.org/10.1038/35039612
Roberts K, Granum E, Leegood RC, Raven JA (2007) Carbon acquisition by diatoms. Photosynth Res 93:79–88. https://doi.org/10.1007/s11120-007-9172-2
Sage RF, Kubien DS (2007) The temperature response of C3 and C4 photosynthesis. Plant Cell Environ 30:1086–1106. https://doi.org/10.1111/j.1365-3040.2007.01682.x
Seabold S, Perktold J (2010) Statsmodels: Econometric and Statistical Modeling with Python. Proc 9th Python Sci Conf. Doi: https://doi.org/10.25080/Majora-92bf1922-011
Sharwood RE, von Caemmerer S, Maliga P, Whitney SM (2008) The catalytic properties of hybrid Rubisco comprising tobacco small and sunflower large subunits mirror the kinetically equivalent source Rubiscos and can support tobacco growth. Plant Physiol 146:83–96. https://doi.org/10.1104/pp.107.109058
Shi D, Hong H, Su X et al (2019) The physiological response of marine diatoms to ocean acidification: differential roles of seawater pCO2 and pH. J Phycol 55:521–533. https://doi.org/10.1111/jpy.12855
Taylor AR (2009) A fast Na+/Ca2+− based action potential in a marine diatom. PLoS One 4:e4966. https://doi.org/10.1371/journal.pone.0004966
Tsuji Y, Mahardika A, Matsuda Y (2017a) Evolutionarily distinct strategies for the acquisition of inorganic carbon from seawater in marine diatoms. J Exp Bot 68:3949–3958. https://doi.org/10.1093/jxb/erx102

Tsuji Y, Nakajima K, Matsuda Y (2017b) Molecular aspects of the biophysical CO2-concentrating mechanism and its regulation in marine diatoms. J Exp Bot 68:3763–3772. https://doi.org/10.1093/jxb/erx173

Virtanen P, Gommers R, Oliphant TE et al (2020) SciPy 1.0: fundamental algorithms for scientific computing in python. Nat Methods 17:261–272. https://doi.org/10.1038/s41592-019-0686-2

Wada S, Agostini S, Harvey BP et al (2021) Ocean acidification increases phytobenthic carbon fixation and export in a warm-temperate system. Estuarine Coastal Shelf Sci 250:107113. https://doi.org/10.1016/j.ecss.2020.107113

Whitney SM, Houtz RL, Alonso H (2011) Advancing our understanding and capacity to engineer nature's CO2-sequestering enzyme, Rubisco. Plant Physiol 155:27–35. https://doi.org/10.1104/pp.110.164814

Woodger FJ, Badger MR, Price GD (2005) Sensing of inorganic carbon limitation in synechococcus PCC7942 is correlated with the size of the internal inorganic carbon pool and involves oxygen. Plant Physiol 139:1959–1969. https://doi.org/10.1104/pp.105.069146

Wu Y, Campbell DA, Irwin AJ et al (2014) Ocean acidification enhances the growth rate of larger diatoms. Limnol Oceanogr 59:1027–1034. https://doi.org/10.4319/lo.2014.59.3.1027

Young JN, Goldman JAL, Kranz SA et al (2015) Slow carboxylation of Rubisco constrains the rate of carbon fixation during Antarctic phytoplankton blooms. New Phytol 205:172–181. https://doi.org/10.1111/nph.13021

Young JN, Heureux AMC, Sharwood RE et al (2016) Large variation in the Rubisco kinetics of diatoms reveals diversity among their carbon-concentrating mechanisms. J Exp Bot 67:3445–3456. https://doi.org/10.1093/jxb/erw163

Zeebe RE (2012) History of seawater carbonate chemistry, atmospheric CO2, and ocean acidification. Annu Rev Earth Planet Sci 40:141–165. https://doi.org/10.1146/annurev-earth-042711-105521